Downloaded from www.ajronline.org by Nathalie Bureau on 06/28/17 from IP address 206.167.168.128. Copyright ARRS. For personal use only; all rights reserved

Carotid Artery Plaque Vulnerability Assessment Using Noninvasive Ultrasound Elastography: Validation With MRI

Marie-Hélène Roy Cardinal[1]
Maarten H. G. Heusinkveld[1,2]
Zhao Qin[1]
Richard G. P. Lopata[2]
Cyrille Naim[1,3]
Gilles Soulez[3,4,5]
Guy Cloutier[1,5]

Keywords: noninvasive vascular elastography, plaque translation motion, strain and shear strain imaging, ultrasound imaging, vulnerable carotid artery plaque

DOI:10.2214/AJR.16.17176

Received August 4, 2016; accepted after revision January 25, 2017.

Supported by grant PPP-78763 from the Canadian Institutes of Health Research (CIHR) and by maturation funding from Univalor, for clinical acquisition of imaging data, and by grants STPGP-381136-09, DG-138570-11, and CHRP-462240-2014 from the Natural Sciences and Engineering Research Council of Canada and grant CPG-134748 from the CIHR, for technical developments and data analyses.

[1]Laboratory of Biorheology and Medical Ultrasonics, University of Montreal Hospital Research Center, 900 St Denis, Rm R11-464, Montreal, QC H2X 0A9, Canada. Address correspondence to G. Cloutier (guy.cloutier@umontreal.ca).

[2]Cardiovascular Biomechanics, Department of Biomedical Engineering, Eindhoven University of Technology, Eindhoven, The Netherlands.

[3]Laboratory of Clinical Image Processing, University of Montreal Hospital Research Center, Montreal, QC, Canada.

[4]Department of Radiology, University of Montreal Hospital, Montreal, QC, Canada.

[5]Department of Radiology, Radio-Oncology, and Nuclear Medicine, and Institute of Biomedical Engineering, University of Montreal, Montreal, QC, Canada.

This article is available for credit.

Supplemental Data
Available online at www.ajronline.org.

AJR 2017; 209:142–151

0361–803X/17/2091–142

© American Roentgen Ray Society

OBJECTIVE. Vulnerable and nonvulnerable carotid artery plaques have different tissue morphology and composition that may affect plaque biomechanics. The objective of this study is to evaluate plaque vulnerability with the use of ultrasound noninvasive vascular elastography (NIVE).

MATERIALS AND METHODS. Thirty-one patients (mean [± SD] age, 69 ± 7 years) with stenosis of the internal carotid artery of 50% or greater were enrolled in this cross-sectional study. Elastography parameters quantifying axial strain, shear strain, and translation motion were used to characterize carotid artery plaques as nonvulnerable, neovascularized, and vulnerable. Maximum axial strain, cumulated axial strain, mean shear strain, cumulated shear strain, cumulated axial translation, and cumulated lateral translations were measured. Cumulated measurements were summed over a cardiac cycle. The ratio of cumulated axial strain to cumulated axial translation was also evaluated. The reference method used to characterize plaques was high-resolution MRI.

RESULTS. According to MRI, seven plaques were vulnerable, 12 were nonvulnerable without neovascularity, and 12 were nonvulnerable with neovascularity (a precursor of vulnerability). The two parameters cumulated axial translation and the ratio of cumulated axial strain to cumulated axial translation could discriminate between nonvulnerable plaques and vulnerable plaques or determine the presence of neovascularity in nonvulnerable plaques (which was also possible with the mean shear strain parameter). All parameters differed between the nonvulnerable plaque group and the group that combined vulnerable plaques and plaques with neovascularity. The most discriminating parameter for the detection of vulnerable neovascularized plaques was the ratio of cumulated axial strain to cumulated axial translation (expressed as percentage per millimeter) (mean ratio, 39.30%/mm ± 12.80%/mm for nonvulnerable plaques without neovascularity vs 63.79%/mm ± 17.59%/mm for vulnerable plaques and nonvulnerable plaques with neovascularity, $p = 0.002$), giving an AUC value of 0.886.

CONCLUSION. The imaging parameters cumulated axial translation and the ratio of cumulated axial strain to cumulated axial translation, as computed using NIVE, were able to discriminate vulnerable carotid artery plaques characterized by MRI from nonvulnerable carotid artery plaques. Consideration of neovascularized plaques improved the performance of NIVE. NIVE may be a valuable alternative to MRI for carotid artery plaque assessment.

The rupture of vulnerable atherosclerotic precerebral and cerebral artery plaques causes stroke. It is estimated that approximately 20–25% of all ischemic strokes are caused by carotid artery atherosclerosis [1]. In the assessment of rupture risk, multicontrast high-resolution MRI has the ability to identify and quantify the carotid artery plaque morphology and its components (e.g., calcifications, lipid-rich necrotic core, intraplaque hemorrhage, fibrous cap thickness, and inflammatory tissue) [2, 3]. A modified American Heart Association (AHA) classification of plaque types for MRI [4] helped to identify high-risk carotid artery atherosclerotic lesions [5]. Plaque characteristics identified with MRI, such as a thin or ruptured fibrous cap, intraplaque hemorrhage, and a large lipid-rich necrotic core, were associated with patients with symptomatic disease [6]. The drawbacks of MRI are increased costs and limited availability.

Duplex ultrasound (US) is commonly used for noninvasive vascular imaging and grading of carotid artery stenoses. Vascu-

Downloaded from www.ajronline.org by Nathalie Bureau on 06/28/17 from IP address 206.167.168.128. Copyright ARRS. For personal use only; all rights reserved

lar US elastography has been proposed as a means of characterizing the vascular wall or plaques of carotid arteries noninvasively [7–13]. Those achievements were inspired by pioneering work in the study of the mechanical properties of coronary artery plaques with intravascular US [14]. With vascular US elastography, mechanical deformations of the vascular wall caused by the blood pressure pulse are estimated and strain images are produced. The shear strain in the adventitia of normal common carotid arteries has also been assessed with US [15]. Carotid elastography has recently been used to differentiate fibrous plaques from atherosclerotic plaques or from plaques with hemorrhage or thrombosis [16]. It has been correlated with neovascularization measured with contrast-enhanced US [17] and with a cognitive performance score [18]. In a review article, most studies found that increased carotid artery stiffness was associated with the presence of carotid artery plaque, the degree of atherosclerosis, and the incidence of stroke [19].

The correlation of carotid artery plaque characteristics between MRI with US-based techniques has been attempted using an echo-tracking system to assess arterial mechanics [20] acoustic radiation force impulse imaging to measure elasticity [21], strain rate [22], and axial strain [23]. The objective of this study is to evaluate the ability of noninvasive vascular elastography (NIVE) to characterize carotid artery plaque vulnerability with MRI used as the reference method. Parameters extracted from elastography sequences of axial strain, shear strain, and translational movement were considered because characterization of heterogeneous plaques could necessitate the use of more than one elastography index. These mechanical parameters describe different components of the 2D deformation of the carotid artery wall caused by natural blood pulsation. Thresholding was applied to these parameters to detect their high magnitudes within the plaques. The elastography parameters were correlated with plaque morphology and composition, including plaque neovascularity, as determined by MRI. It was hypothesized that the new mechanical parameters would enable NIVE to discriminate between stable and vulnerable carotid artery plaques.

Materials and Methods

Study Population

Thirty-one patients (22 men and nine women) were enrolled in this cross-sectional study performed at the Centre Hospitalier de l'Université de Montréal. This population had been the focus of a previous report [23]. Written informed consent was obtained from each patient. The protocol conformed to the ethical guidelines of the Declaration of Helsinki, and the study was approved by the institutional review board on ethics at the Centre Hospitalier de l'Université de Montréal.

Inclusion criteria were patient age between 40 and 90 years and carotid artery stenosis of 50% or greater. Exclusion criteria were the presence of severe calcification and previous radiotherapy of the neck region, endarterectomy, or carotid artery stenting. The mean (± SD) age of participants was 69 ± 7 years. A subgroup of nine patients with symptomatic disease (seven men and two women) had experienced cerebral events (either ischemic stroke or a transient ischemic attack) in the 3 months before examination. In all patients with symptomatic disease, the presence of a plaque at the ipsilateral internal carotid artery was associated with the cerebral event that occurred. The remaining 22 patients (15 men and seven women) with carotid artery stenosis of 50% or greater were considered to have asymptomatic disease. The percentage of stenosis was documented by a radiology resident on the basis of findings from a previous angiographic study, if available (19 patients had undergone CT angiography, whereas three had undergone MR angiography and one had undergone digital subtraction angiography), combined with findings from duplex Doppler US, or solely on the basis of duplex US using standard criteria (for eight patients) [24]. For angiographic studies, stenosis was evaluated according to the criteria of the North American Symptomatic Carotid Endarterectomy Trial [25].

MRI

With the use of a 1.5-T MRI unit (Avanto, Siemens Healthcare) and a dedicated four-element radiofrequency (RF) surface coil, cross-sectional images of the index carotid artery were obtained from 1 cm below to 3 cm above the bifurcation. A 3D time-of-flight sequence was performed. With the patient kept in the same position and with use of a voxel size of 0.6 × 0.5 × 3 mm^3 with a 1-mm intersection gap, four black-blood double inversion recovery turbo spin-echo sequences were acquired in the following order: T2-weighted imaging, proton density–weighted imaging, and unenhanced and contrast-enhanced T1-weighted imaging. Two adjacent slices containing the major portion of the plaque were selected for contrast-enhanced imaging. After gadobenate dimeglumine (MultiHance, Bracco Diagnostics) was administered, image acquisition was performed every minute for 10 minutes. The total imaging time was typically less than 45 minutes.

All image sequences were used for interpretation of plaque components and plaque segmentation. At each image slice level, vessel contours and components were manually traced using segmentation software (QPlaque MR 1.0.16, Medis) that provided volume and area measurements [26]. Delineated plaque components included the lipid-rich necrotic core, calcifications, neovascularity, intraplaque hemorrhage, and the fibrous cap. The lipid core was generally located in the bulk of the plaque and showed isointense to hyperintense signal on T1-weighted and proton density–weighted images and hypointense signal on T2-weighted images [27]. Calcification was characterized by areas of hypointense signal on all four weightings [27]. Neovascularization was defined by the presence of contrast enhancement (increase in signal intensity of at least 30%) on the contrast-enhanced image sequence. The contrast-enhanced image sequence chosen for analysis was acquired at least 5 minutes after the initiation of contrast injection and displayed the best image quality and maximum enhancement. Intraplaque hemorrhage was identified as hyperintense signal on T1-weighted and time-of-flight imaging [3, 28]. A thin or ruptured cap was visualized on T1-weighted, T2-weighted, proton density–weighted, and time-of-flight images [29]. The volume percentage of plaque components was calculated with respect to the total wall volume. Volumes were computed as the sum of the segmentation areas on all slices multiplied by the slice thickness. The maximum area of plaque components on all cross-sectional images was computed and was expressed as a percentage value and as millimeters squared, for the lipid core and calcifications. Furthermore, a generic characterization of the plaque was performed on the basis of the Conventional and Modified AHA Classification of Atherosclerotic Plaque [4], types IV–V to VIII.

Plaque vulnerability characteristics based on MRI findings from all cross-sectional images were assessed by a radiology resident. Plaque images were then reviewed by a radiologist with 25 years of experience in vascular MRI. The carotid artery plaque was deemed vulnerable in cases of a thin fibrous cap with a large (surface area, > 25%) lipid core, a ruptured fibrous cap, or intraplaque hemorrhage. The presence of intraplaque hemorrhage, a lipid core, and thinning or rupture of the fibrous cap on MR images of carotid artery plaques has been associated with an increased risk of future stroke or transient ischemic attack [30]. In the present study, we distinguished between nonvulnerable plaques with and without neovascularity because neovascularity is a precursor of vulnerability [31] and because, when assessed by contrast-enhanced MRI, neovascularity was associated with patients with symptomatic disease and with vulnerable plaques as defined by histologic findings [32].

Downloaded from www.ajronline.org by Nathalie Bureau on 06/28/17 from IP address 206.167.168.128. Copyright ARRS. For personal use only; all rights reserved

Ultrasound Acquisitions

Two-dimensional duplex US recordings in the longitudinal view of the carotid artery were acquired with an HDI 5000 US system (Philips Healthcare), with the use of an L7–4 linear array probe. The aim of this examination was to identify the diseased artery segment and grade the severity of the stenosis. RF echo data acquisitions were then performed by the same experienced radiologist who reviewed the plaque images, with the use of a US research system (ES500RP, Ultrasonix) equipped with an L14–5/38 linear array transducer (with 128 elements and 7.2-MHz center frequency with a fractional bandwidth of 70% at –6 dB). RF data were sampled at 40 MHz. B-mode sequences were reconstructed from acquired RF data; the frame rate for both B-mode and RF data was 19–25 Hz. The plaque area was segmented from B-mode sequences with the use of an automated method [33] and was verified by the experienced radiologist before elastogram computation was done; the segmentation algorithm for carotid artery plaque was validated with a different population.

Noninvasive Vascular Elastography

The elastography analysis was performed by a graduate student supervised by a research associate. Both were blinded to the MRI analysis. Elastograms were computed for the whole sequence of each segmented plaque [7, 9]. We used an implementation of NIVE integrated into a commercial imaging platform (Visual, Object Research Systems) [23, 34]. The NIVE technique estimates 2D displacement maps of a carotid artery plaque between consecutive frames and thus provides axial and lateral translations along with strain and shear strain images (with "axial" indicating the direction along the US beam and "lateral" indicating the direction perpendicular to the axial direction). Translations are rigid displacements produced by the pulsating blood pressure. An axial strain indicates a compression or dilation along the direction of the US beam during the cardiac cycle. A shear strain corresponds to an angular change of shape. An angulated deformation can be caused by the heterogeneity of the plaque that does not necessarily move axially when subjected to a radial pressure and by the flow that is producing a tangential movement of the plaque, especially when entering into a severe stenosis [34]. More details about the elastography method that was used can be found in Appendix S1 (which can be viewed in the *AJR* electronic supplement to this article, available at www.ajronline.org). Axial and lateral translations, axial strains, and shear strains are schematically illustrated in Fig. S2.

Postprocessing

For the aforementioned NIVE 2D maps, instantaneous measures consisted of values spatially averaged over the whole segmented plaque of a single elastogram frame. Time-varying curves were obtained by computing instantaneous parameters over the whole sequence (Figs. S3 and S4, supplemental images, which can be viewed in the *AJR* electronic supplement to this article, available at www.ajronline.org). Cumulative curves were computed by adding instantaneous measures over separate cardiac cycles (i.e., values were reset to zero at each cycle). Descriptive indexes were extracted from these curves: mean absolute shear strain, cumulated absolute shear strain, maximum axial strain, cumulated axial strain, cumulated axial translation, cumulated lateral translation, and the ratio of the cumulated axial strain to the cumulated axial translation. Cumulative parameters were defined as the range (maximum value to minimum value) during a cardiac cycle. All descriptive indexes were extracted from all available cardiac cycles (mean, 5 ± 1 cycles) and were then averaged. Cardiac cycles were selected manually (Figs. S3 and S4).

Thresholds were also applied on the elastogram 2D maps to identify plaque areas containing high translation, strain, or shear strain values, thus emphasizing large mechanical movements. This image processing strategy is similar to approaches used in strain imaging [11] and in obtaining in vitro strain data from inflation testing [13]. Pixel areas containing 25% of the highest values of each parameter were selected and displayed as instantaneous or cumulative time-varying curves (the 75th percentile of each individual elastogram frame was chosen). Outlier values were winsorized before thresholding and averaging was done [35]. The 25% threshold was predetermined arbitrarily.

Statistical Analysis

Elastography parameters are presented as mean (± SD) values. All statistical analyses were performed using statistical software (R, version 3.2.5, R Foundation). Data were tested for normality with the use of a Shapiro-Wilk test. Parametric and nonparametric ANOVA with pairwise multiple comparisons were performed to evaluate differences between plaque groups. Spearman correlation coefficients were computed between elastography parameters and blood pressure measurements. ANOVA tests were conducted to evaluate the statistical significance of linear regression analyses between elastography indexes and plaque components (i.e., lipid core, calcium, and neovasculature) and the percentage of stenosis. The p values were adjusted using the Holm-Bonferroni method for multiple testing in ANOVA and linear regression analyses. A $p \leq 0.05$ was considered to denote statistical significance. ROC curves were generated to determine sensitivity and specificity in discriminating between MRI-based plaque groups. Ten thousand bootstrap replications of each index were used to compute the CI of the areas under the curve.

Results

The clinical characteristics of patients with asymptomatic and symptomatic disease are presented in Table 1. Imaging of the left internal carotid artery was performed for 13 patients, whereas imaging of the right internal carotid artery was done for the remaining 18 patients. Only the ipsilateral side was chosen for patients with symptomatic disease, and the side with the most severe stenosis was considered for the group with asymptomatic disease. For five patients, a plaque was only present and segmented at either the far or near wall of the carotid artery.

Seven plaques were deemed vulnerable on MRI, 12 plaques appeared nonvulnerable without neovascularization, and 12 plaques were nonvulnerable but contained neovascularity. MRI plaque component characteristics are also presented in Table 1. Additional clinical characteristics and technical parameters for this plaque grouping are presented in Table S5 (which can be viewed in the *AJR* electronic supplement to this article, available at www.ajronline.org). No difference was found in the pressure gradient between consecutive US images between groups (i.e., there was no confounding effect on differences in the elastography indexes between groups). However, a statistically significant correlation was found between thresholded cumulated axial strains and the blood pressure gradient between consecutive image frames (Spearman correlation = –0.37, $p = 0.044$); no correlation was found with the other elastography indexes (with or without thresholding). The pressure gradient was estimated by considering the US frame rate, the heart rate, and the systolic and diastolic blood pressures [9]. No correlation was found between elastography indexes and the pulse pressure (i.e., the difference between systolic and diastolic blood pressures).

Fig. 1A shows an example of a B-mode image of a vulnerable plaque with a superimposed axial shear strain map. Small regions near the vessel lumen contained high shear values and appeared as red areas on the color map. Figs. 1B and 1C present examples of the cumulated axial strain and cumulated axial translation for that plaque. Examples of time-varying curves of the shear strain and axial strain are presented in Fig. S3, whereas those of the axial and lateral translations are shown in Fig. S4.

Downloaded from www.ajronline.org by Nathalie Bureau on 06/28/17 from IP address 206.167.168.128. Copyright ARRS. For personal use only; all rights reserved

As shown in Table 2, thresholded cumulated axial translations and the ratios of the cumulated axial strain to the cumulated axial translation were statistically significantly different between patients with a vulnerable plaque and a nonvulnerable plaque without neovascularization. Statistically significant differences were also found between mean shear strains, thresholded cumulated axial translation, and the thresholded ratio of the cumulated axial strain to the cumulated axial translation, for the comparison of nonvulnerable plaques with and without neovascularity. In general, thresholded elastograms of all indexes were more discriminating (i.e., had lower *p* values), except for shear strain parameters (i.e., mean shear strain and cumulated shear strain).

Because neovascularization is a precursor of plaque vulnerability [31], nonvulnerable plaques with neovascularization and vulnerable plaques were grouped together and were compared with nonvulnerable plaques without neovascularity (Table 3). All elastography parameters could discriminate between these two new groups (p = 0.002–0.028). Linear regressions showed no correlation between these parameters and the percentage of stenosis (Table S6 can be viewed in the *AJR* electronic supplement to this article, available at www.ajronline.org).

Grouping vulnerable plaques with the ones containing neovascularity increased the power of statistical tests for all parameters (Table 3). The most discriminating parameters were the mean shear strain of the whole plaque (without thresholding), the cumulated axial translation (with thresholding), and the ratio of the cumulated axial strain to the cumulated axial translation (also with thresholding). ROC curves based on those indexes were generated to determine their sensitivity and specificity in the detection of plaques at risk according to MRI (Fig. 2).

Cumulated shear strains and thresholded maximum axial strains of complex plaques with a possible surface defect, hemorrhage, or thrombus (AHA category VI) were different from other AHA plaque categories (Table 4). Other elastography parameters could not differentiate between plaque categories according to the AHA classification. We also found a statistically significant positive linear correlation ($R^2 = 0.418$, $p = 0.006$) (Fig. 3) between the cumulated shear strain (without thresholding) and the maximum calcium area. Correlations between other plaque components and elastography parameters are presented in Table S7 (which can be viewed in the *AJR* electronic supplement to this article, available at www.ajronline.org).

TABLE 1: Overview of Relevant Clinical Parameters Derived from Clinical, Ultrasound, and MRI Examinations

Parameter	Patients With Asymptomatic Disease (n = 22)	Patients With Symptomatic Disease (n = 9)	p
Age (y), mean ± SD	69.3 ± 7.5	69.3 ± 9.0	0.99[a]
Carotid artery side			0.11[b]
Left internal carotid artery	7	6	
Right internal carotid artery	15	3	
Stenosis percentage			
Mean ± SD	72 ± 12	74 ± 12	0.72[c]
50–69%	7	2	0.69[d]
70–90%	15	7	
MRI plaque dimension			
Area (mm^2), mean ± SD	77 ± 42	101 ± 76	0.50[a]
Volume (mm^3), mean ± SD	1500 ± 642	1598 ± 792	0.72[c]
Modified AHA classification[e]			0.02[b]
IV–V	7	3	
VI	1	4	
VII	9	0	
VIII	5	2	
MRI-defined plaque status			0.16[d]
Nonvulnerable without neovascularity	10	2	
Nonvulnerable with neovascularity	8	4	
Vulnerable	4	3	
Lipid			
Present	10	7	0.132[d]
Volume (%), mean ± SD	3.0 ± 7.9	9.4 ± 11.3	0.024[a]
Maximum area (%), mean ± SD	9.1 ± 14.7	20.0 ± 14.7	0.047[a]
Maximum area (mm^2), mean ± SD	4.6 ± 8.5	16.4 ± 15.8	0.019[a]
Calcium			
Present	19	8	> 0.999[d]
Volume (%), mean ± SD	6.3 ± 4.8	2.2 ± 2.5	0.024[c]
Maximum area (%), mean ± SD	13.8 ± 8.7	6.6 ± 5.0	0.027[c]
Maximum area (mm^2), mean ± SD	9.3 ± 7.8	4.3 ± 4.2	0.139[a]
Neovascularity			
Present	13	6	> 0.999[d]
Volume (%), mean ± SD	1.8 ± 2.3	3.0 ± 4.0	0.654[a]
Intraplaque hemorrhage			
Present	0	2	0.077[d]
Volume (%), mean ± SD	0.0 ± 0.0	0.2 ± 0.3	0.028[a]
Fibrous tissue			
Volume (%), mean ± SD	87.4 ± 8.0	84.4 ± 12.3	0.913[a]

Note—Except where otherwise indicated, data are number of patients. Volumes and maximum areas of plaque components were determined from analysis of MR images. AHA = American Heart Association.
[a]Mann-Whitney *U* test.
[b]Pearson chi-square test.
[c]*t* test.
[d]Fisher exact test.
[e]Plaques were characterized according to the AHA classifications.

Downloaded from www.ajronline.org by Nathalie Bureau on 06/28/17 from IP address 206.167.168.128. Copyright ARRS. For personal use only; all rights reserved

TABLE 2: Overview of Elastography Indexes Obtained for Plaques Identified on MRI as Vulnerable, Nonvulnerable With Neovascularity, and Nonvulnerable Without Neovascularity

Strain Parameter and Threshold[a]	Vulnerable Plaques ($n = 7$)	Nonvulnerable Plaques With Neovascularity ($n = 12$)	Nonvulnerable Plaques Without Neovascularity ($n = 12$)	p[b]		
				Vulnerable Plaques vs Nonvulnerable Plaques With Neovascularity	Vulnerable Plaques vs Nonvulnerable Plaques Without Neovascularity	Nonvulnerable Plaques With Neovascularity vs Nonvulnerable Plaques Without Neovascularity
Mean shear strain magnitude (%)						
Yes	0.54 ± 0.14	0.52 ± 0.13	0.69 ± 0.14	1	0.275	0.085
No	0.24 ± 0.06	0.23 ± 0.06	0.32 ± 0.07	1	0.154	0.042[c]
Cumulated shear strain magnitude (%)						
Yes	12.91 ± 4.80	11.97 ± 2.89	16.22 ± 3.82	1	0.414	0.112
No	5.56 ± 1.78	5.24 ± 1.24	7.17 ± 1.79	1	0.486	0.108
Maximum axial strain (%)						
Yes	1.95 ± 0.51	1.98 ± 0.44	2.34 ± 0.39	1	0.452	0.202
No	0.47 ± 0.16	0.50 ± 0.15	0.54 ± 0.13	1	1	> 0.999
Cumulated axial strain (%)						
Yes	16.23 ± 5.28	15.19 ± 2.81	19.90 ± 4.57	1	0.280	0.112
No	1.57 ± 0.59	1.80 ± 0.65	1.91 ± 0.55	1	1	> 0.999
Cumulated axial translation (mm)						
Yes	0.25 ± 0.09	0.29 ± 0.17	0.58 ± 0.29	1	0.03[c]	0.042[c]
No	0.24 ± 0.11	0.26 ± 0.17	0.44 ± 0.29	1	0.620	0.670
Cumulated lateral translation (mm)						
Yes	0.70 ± 0.48	0.82 ± 0.68	1.30 ± 0.53	1	0.452	0.202
No	0.28 ± 0.18	0.33 ± 0.24	0.52 ± 0.30	1	0.620	0.670
Ratio of cumulated axial strain to cumulated axial translation (%/mm)						
Yes	67.7 ± 14.2	61.50 ± 19.50	39.30 ± 12.80	1	0.02[c]	0.028[c]
No	7.21 ± 3.25	9.55 ± 5.08	6.50 ± 5.32	1	1	> 0.999

Note—Except where otherwise indicated, data are mean (± SD) values.

[a] "Yes" denotes indexes obtained from plaque regions containing 25% of the highest values, and "no" denotes indexes averaged over the whole plaque region.

[b] One-way ANOVA with multiple comparisons and use of the Holm-Bonferroni adjustment method for multiple testing.

[c] Statistically significant difference ($p < 0.05$).

Downloaded from www.ajronline.org by Nathalie Bureau on 06/28/17 from IP address 206.167.168.128. Copyright ARRS. For personal use only; all rights reserved

TABLE 3: Overview of Elastography Indexes Obtained for the Combined Group of Vulnerable Plaques and Nonvulnerable Plaques With Neovascularity Compared With Nonvulnerable Plaques Without Neovascularity

Strain Parameter	Threshold[a]	Vulnerable Plaques and Nonvulnerable Plaques With Neovascularity (n = 19)	Nonvulnerable Plaques Without Neovascularity (n = 12)	p[b]
Mean shear strain magnitude (%)	No	0.23 ± 0.06	0.32 ± 0.07	0.004
Cumulated shear strain magnitude (%)	No	5.35 ± 1.42	7.17 ± 1.79	0.016
Maximum axial strain (%)	Yes	1.97 ± 0.46	2.34 ± 0.39	0.028
Cumulated axial strain (%)	Yes	15.58 ± 3.79	19.90 ± 4.57	0.016
Cumulated axial translation (mm)	Yes	0.27 ± 0.14	0.58 ± 0.29	0.003
Cumulated lateral translation (mm)	Yes	0.77 ± 0.60	1.30 ± 0.53	0.016
Ratio of cumulated axial strain to cumulated axial translation (%/mm)	Yes	63.79 ± 17.59	39.30 ± 12.80	0.002

Note—Except where otherwise indicated, data are mean (± SD) values.
[a]"Yes" denotes indexes obtained from plaque regions containing 25% of the highest values, and "no" denotes indexes averaged over the whole plaque region.
[b]Statistically significant difference ($p < 0.05$, t test using the Holm-Bonferroni adjustment method for multiple testing) between both groups.

Discussion

This pilot study resulted in the following findings: NIVE indexes could identify vulnerable plaques as validated by MRI, and the presence of neovascularization amplified the discriminating power of US; thresholding elastography maps generally improved the performance of this method; and with the exception of the ratio of the cumulated axial strain to the cumulated axial translation, all elastography indexes had lower magnitude in vulnerable plaques, and this latter category had values similar to those of nonvulnerable plaques with neovascularization.

The concept of reconstructing time-varying curves from elastography images acquired over multiple cardiac cycles, followed by parameter estimations, has been reported in similar studies [9, 10, 18]. We previously used this approach of averaging the axial strain over the entire segmented plaque to detect a lipid pool [23]. It was applied to the axial strain only without analyzing the influence of plaque neovascularity on elastography parameters; thus, vulnerable plaques could not be distinguished from nonvulnerable plaques.

Table 2 shows similar results for the maximum axial strain and cumulated axial strain. Our objective was to analyze areas of the plaque that exhibited high strains, shears, and translations instead of averaging this information with other image pixels depicting low magnitudes. With thresholding, maximum axial strain, cumulated axial strain, cumulated axial translation, cumulated lateral translation, and the ratio of cumulated axial strain to cumulated axial translation could better discriminate vulnerable plaques or nonvulnerable neovascularized plaques from nonvulnerable plaques without neovascularization (Table 3). Shear strain indexes (mean shear strain and cumulated shear strain) averaged over the whole plaque could provide a better differentiation of these groups. It should be noted that statistically significant differences were found between the thresholded shear strain indexes (mean shear strain and cumulated shear strain) of the combined group of vulnerable and neovascularized plaques versus nonvulnerable plaques without neovascularization (but with worse discrimination noted at higher p values of 0.015 and 0.024; data not shown).

The best ROC accuracies were obtained with the parameters cumulated axial translation and the ratio of the cumulated axial strain to the cumulated axial translation. We did not consider the position and pattern of pixels exhibiting high magnitudes; this could be investigated in a future study. We tested other thresholds (50% and 10% of the highest values), and similar results were obtained (data not shown). The 25% threshold was thus a good compromise to study high deformations without excluding too much plaque area.

Most carotid artery elasticity studies in the literature have found increased stiffness with the degree of atherosclerosis, the presence of carotid artery plaque, and the incidence of stroke [19]. We have also previously measured lower axial strain indexes in atherosclerotic carotid arteries, compared with normal ones [34]. Findings from that previous study are in line with our observations in the present study. Indeed, lower mean deformations and translational movements were found in patients with a vulnerable or a neovascularized plaque (Tables 2 and 3). In the present study, lower axial shear strains (mean shear strain and cumulated shear strain) were also found in vulnerable and neovascularized plaques, compared with nonvulnerable plaques free of neovascularity. Lower shear strains represent less angular deformation of

TABLE 4: Cumulated Shear Strain Magnitude and Maximum Axial Strain Elastography Indexes for American Heart Association (AHA) Plaque Classifications IV–V, VI, VII, and VIII as Based on MRI

Strain Parameter	Threshold[a]	Modified AHA Plaque Classification			
		IV–V (n = 10)	VI (n = 5)	VII (n = 9)	VIII (n = 7)
Cumulated shear strain magnitude (%)	No	6.30 ± 1.72	4.65 ± 1.38[b]	7.24 ± 1.94	5.20 ± 0.75
Maximum axial strain (%)	Yes	2.24 ± 0.38	1.53 ± 0.31[c]	2.23 ± 0.37	2.19 ± 0.52

Note—Except where otherwise indicated, data are mean (± SD) values.
[a]"Yes" denotes indexes obtained from plaque regions containing 25% of the highest values, and "no" denotes indexes averaged over the whole plaque region.
[b]Significant difference between AHA classifications VI and VII (p = 0.022, one-way ANOVA).
[c]Significant difference compared with the other groups (p = 0.013, one-way ANOVA).

Downloaded from www.ajronline.org by Nathalie Bureau on 06/28/17 from IP address 206.167.168.128. Copyright ARRS. For personal use only; all rights reserved

the plaque geometry (Fig. S2). In one study, relative strain, which was computed from an elastography tissue hardness score, was found to be higher for fibrous plaques than for atherosclerotic plaques or plaques with hemorrhage or thrombosis [16]. In addition, lower peak axial strains and shear strains were observed for patients with symptomatic disease (*p* values not provided) [18]. Nevertheless, Huang et al. [22] recently found that the strain rate was significantly higher in vulnerable plaques identified by MRI than in stable plaques and that intraplaque neovascularization measured with contrast-enhanced US was associated with higher axial strain values [17]. Note that the average stenosis percentage in the study by Huang and colleagues was approximately 30%, compared with more than 70% in the present study.

It has generally been observed in US elastography studies that the soft lipid pool within vulnerable plaques (i.e., the coronary, femoral, and carotid arteries) exhibits higher strain values than does calcified stiffer tissue [11, 14, 36] or that hard plaque regions have lower axial strain values than do normal wall regions [7]. With the use of acoustic radiation force impulse imaging, increased displacements have been measured in regions identified as lipid with MRI [21]. However, no correlation has been found between strain features and the lipid core size [17]. In the present study, reduced elastography indexes (or an increase in the case of the ratio of the cumulated axial strain to the cumulated axial translation) were noticed for vulnerable plaques or plaques with neovascularization. This may be explained by our database of patients with fibrotic plaques with no prominent evidence of large lipid pools (mean lipid volume based on MRI, 9.6% ± 12.5% and 5.9% ± 10.8% for the vulnerable plaque group and the nonvulnerable but neovascularized plaque group, respectively).

A few reports have studied carotid artery plaque translation in advanced atherosclerosis [37, 38]. Our study concluded that cumulated axial and lateral translations could identify vulnerable and neovascularized plaques (Table 3). By combining the cumulated axial strain with the cumulated axial translation to obtain a ratio of the two parameters, optimum discrimination was achieved (Fig. 2). The higher ratio of the cumulated axial strain to the cumulated axial translation in vulnerable and neovascularized plaques can be explained by the greater decrease in axial translation values (i.e., a reduction in cumulated axial translation of 53%) compared with axial strain values (i.e., a reduction in cumulated axial strain of 22%) in those patients. This ratio could be seen as a normalization procedure used to account for the lesser motion observed in vulnerable plaques. In previous studies, low longitudinal displacement of the common carotid artery assessed with US was associated with greater occurrence of myocardial ischemia [37] and with established cardiovascular risk factors [38].

The lower axial shear strains in vulnerable and neovascularized plaques seem to contradict intravascular US results of an animal study in which a positive correlation was found between mean axial shear strains and plaque severity (i.e., AHA score) [39]. However, reduced strains evaluated with an echo-tracking system were also observed in complex plaques (AHA classifications IV–VIII vs AHA classifications I–III) [20]. As noticed in Table 4, no linear trends were observed between cumulated shear strains and AHA plaque classifications. However, in a study by Majdouline et

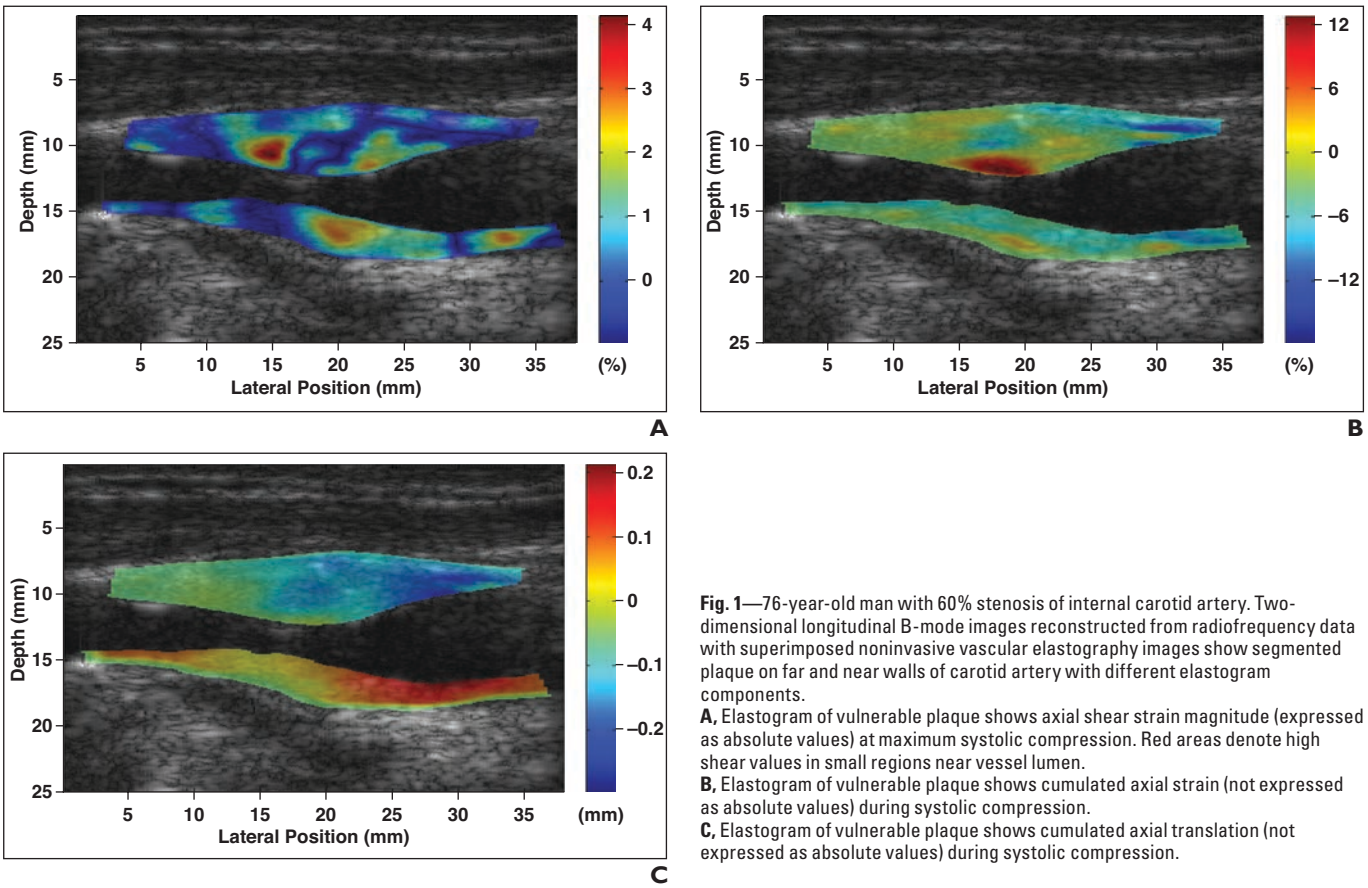

Fig. 1—76-year-old man with 60% stenosis of internal carotid artery. Two-dimensional longitudinal B-mode images reconstructed from radiofrequency data with superimposed noninvasive vascular elastography images show segmented plaque on far and near walls of carotid artery with different elastogram components.
A, Elastogram of vulnerable plaque shows axial shear strain magnitude (expressed as absolute values) at maximum systolic compression. Red areas denote high shear values in small regions near vessel lumen.
B, Elastogram of vulnerable plaque shows cumulated axial strain (not expressed as absolute values) during systolic compression.
C, Elastogram of vulnerable plaque shows cumulated axial translation (not expressed as absolute values) during systolic compression.

Downloaded from www.ajronline.org by Nathalie Bureau on 06/28/17 from IP address 206.167.168.128. Copyright ARRS. For personal use only; all rights reserved

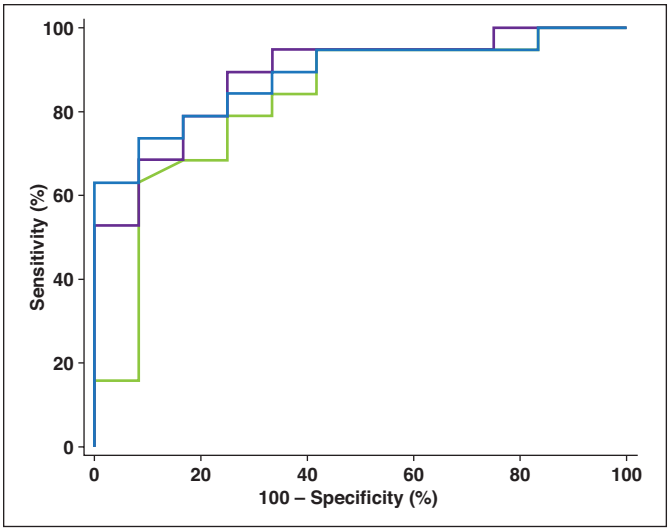

Fig. 2—Comparison of elastography indexes. ROC curve analysis shows sensitivity and specificity of mean shear strain magnitude (*green curve*) (AUC value, 82.7%; 95% CI, 64.7–96.5%), cumulated axial translation (*purple curve*) (AUC value, 88.6%; 95% CI, 75.0–98.3%), and ratio of cumulated axial strain to cumulated axial translation (*blue curve*) (AUC value, 88.6%; 95% CI, 75.0–98.3%) in detection of vulnerable plaques or plaques with neovascularization.

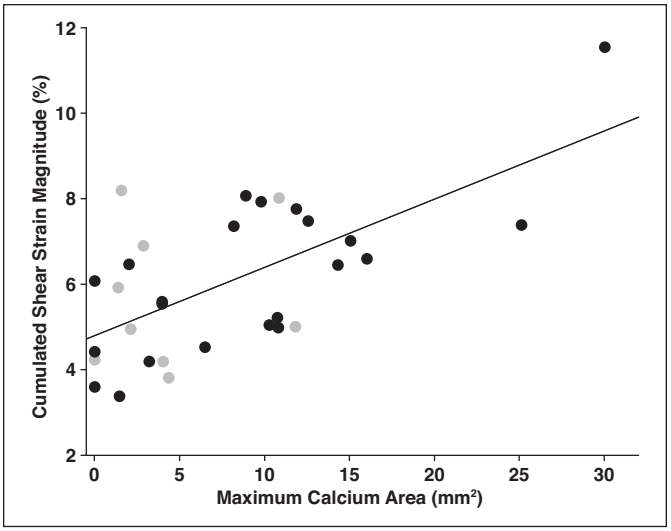

Fig. 3—Association between cumulated shear strain magnitude and maximum calcium area in patients with symptomatic disease (*gray circles*) and patients with asymptomatic disease (*black circles*) measured by MRI. Scatterplot shows statistically significant positive linear correlation ($R^2 = 0.418$; $p = 0.006$; $y = 4.81 + 0.16x$).

al. [39], plaques were defined as AHA classifications I–V on the basis of histologic analysis, whereas more advanced plaques (MRI classifications IV–V to VIII) were included in the current analysis. This prevents direct comparison of results because complex plaques are difficult to find in animal models [40].

In another intravascular US elastography study by Keshavarz-Motamed et al. [41], coronary artery plaque shear strains increased with the soft plaque content of excised lesions, but no correlations were noted between the lipid plaque content measured with MRI and any elastography indexes, including the shear strain (Table S7). Note that the percentage of areas of soft plaque content ranged from 40% to 90% in the study by Keshavarz-Motamed and colleagues [41], compared with a range of 0–50% in the present study (only eight plaques had a lipid core maximum area larger than 20%). In the present study, correlations between MRI-defined plaque components and elastography parameters were made even though cross-sectional MR images were not registered with longitudinal US images (Table S7); this limitation should be addressed in future studies by developing 3D US NIVE methods.

In the current study, MRI was used to identify vulnerable plaques and quantify their tissue components. Although histologic analysis after atherectomy is the reference standard for plaque vulnerability assessment, MRI was chosen to characterize plaques because our study included patients with asymptomatic disease who did not undergo surgery. Plaque characterization with MRI is reproducible, but significant variability was noted, particularly for lipid core and fibrous cap identification with interobserver agreements (kappa values) of 0.58 and 0.28, respectively; a moderately better agreement ($\kappa = 0.62$) was achieved for plaque hemorrhages [42]. However, it was also found more recently that fibrous cap thickness, in addition to lipid core and calcified plaque areas from low- and high-resolution MRI scans of carotid artery plaques, was not significantly different [43]. Moreover, the intraclass correlation coefficient of scans and rescans was 0.58 for lipid core with high-resolution MRI; for other plaque components, intraclass correlation coefficients were greater than 0.75. For comparison, variability in axial strain measurements obtained with NIVE was reported for normal carotid artery wall acquisitions, and intraclass correlation coefficients of 0.72 and 0.52 between two operators were obtained for common and internal carotid arteries, respectively [9]. It was also observed that axial strain parameters were not statistically significantly different between plaques on the far and near walls of internal carotid arteries [34].

The first limitation of the present study is its limited sample size of 31 carotid artery plaques. Elastograms of vulnerable and nonvulnerable plaques were compared, but the predictive value of elastography for plaque rupture was not investigated. Blood pressure was not a confounding factor in the present study; however, testing for the potential confounding impact of blood pressure would be important in future vascular elastography studies. Elastography measures were computed offline because, to our knowledge, NIVE has not yet been implemented on clinical scanners; visual feedback of elastograms thus was not available during acquisition. The quality of elastography images thus could not be optimized during scanning because RF data acquisitions were performed and then imported in our elastography imaging platform for analysis. Severe calcifications were excluded because signal loss would impact elastography measures. Finally, because 2D longitudinal images of the carotid artery were analyzed, out-of-plane motion artifacts were inevitable. The extension of the NIVE method to 3D US images could provide a more complete characterization of plaques.

In conclusion, NIVE provides insight regarding in vivo mechanical imaging of carotid artery plaques in patients and is able to detect vulnerable and neovascularized plaques on the basis of lower axial strains, shear strains, axial and lateral translations and a higher ratio of the cumulated axial strain to the cumulated axial translation. With additional validation, this technology, when added to duplex Doppler US, may be an alternative to costly MRI in the assessment of carotid artery plaques for stroke prevention.

Downloaded from www.ajronline.org by Nathalie Bureau on 06/28/17 from IP address 206.167.168.128. Copyright ARRS. For personal use only; all rights reserved

References

1. Pasternak RC, Criqui MH, Benjamin EJ, et al. Atherosclerotic vascular disease conference: writing group I—epidemiology. *Circulation* 2004; 109:2605–2612
2. Cai J, Hatsukami TS, Ferguson MS, et al. In vivo quantitative measurement of intact fibrous cap and lipid-rich necrotic core size in atherosclerotic carotid plaque: comparison of high-resolution, contrast-enhanced magnetic resonance imaging and histology. *Circulation* 2005; 112:3437–3444
3. Cappendijk VC, Cleutjens KB, Kessels AG, et al. Assessment of human atherosclerotic carotid plaque components with multisequence MR imaging: initial experience. *Radiology* 2005; 234:487–492
4. Cai JM, Hatsukami TS, Ferguson MS, Small R, Polissar NL, Yuan C. Classification of human carotid atherosclerotic lesions with in vivo multicontrast magnetic resonance imaging. *Circulation* 2002; 106:1368–1373
5. Esposito-Bauer L, Saam T, Ghodrati I, et al. MRI plaque imaging detects carotid plaques with a high risk for future cerebrovascular events in asymptomatic patients. *PLoS One* 2013; 8:e67927
6. Millon A, Mathevet JL, Boussel L, et al. High-resolution magnetic resonance imaging of carotid atherosclerosis identifies vulnerable carotid plaques. *J Vasc Surg* 2013; 57:1046-1051.e2
7. Schmitt C, Soulez G, Maurice RL, Giroux MF, Cloutier G. Noninvasive vascular elastography: toward a complementary characterization tool of atherosclerosis in carotid arteries. *Ultrasound Med Biol* 2007; 33:1841–1858
8. Ribbers H, Lopata RG, Holewijn S, Pasterkamp G, Blankensteijn JD, de Korte CL. Noninvasive two-dimensional strain imaging of arteries: validation in phantoms and preliminary experience in carotid arteries in vivo. *Ultrasound Med Biol* 2007; 33:530–540
9. Maurice RL, Soulez G, Giroux MF, Cloutier G. Noninvasive vascular elastography for carotid artery characterization on subjects without previous history of atherosclerosis. *Med Phys* 2008; 35:3436–3443
10. Shi H, Mitchell CC, McCormick M, Kliewer MA, Dempsey RJ, Varghese T. Preliminary in vivo atherosclerotic carotid plaque characterization using the accumulated axial strain and relative lateral shift strain indices. *Phys Med Biol* 2008; 53:6377–6394
11. McCormick M, Varghese T, Wang X, Mitchell C, Kliewer M, Dempsey R. Methods for robust in vivo strain estimation in the carotid artery. *Phys Med Biol* 2012; 57:7329–7353
12. Lopata RG, Peters MF, Nijs J, Oomens CW, Rutten MC, van de Vosse FN. Vascular elastography: a validation study. *Ultrasound Med Biol* 2014; 40:1882–1895
13. Boekhoven RW, Rutten MC, van Sambeek MR, van de Vosse FN, Lopata RG. Towards mechanical characterization of intact endarterectomy samples of carotid arteries during inflation using Echo-CT. *J Biomech* 2014; 47:805–814
14. de Korte CL, Pasterkamp G, van der Steen AF, Woutman HA, Bom N. Characterization of plaque components with intravascular ultrasound elastography in human femoral and coronary arteries in vitro. *Circulation* 2000; 102:617–623
15. Idzenga T, Holewijn S, Hansen HH, de Korte CL. Estimating cyclic shear strain in the common carotid artery using radiofrequency ultrasound. *Ultrasound Med Biol* 2012; 38:2229–2237
16. Liu F, Yong Q, Zhang Q, Liu P, Yang Y. Real-time tissue elastography for the detection of vulnerable carotid plaques in patients undergoing endarterectomy: a pilot study. *Ultrasound Med Biol* 2015; 41:705–712
17. Zhang Q, Li C, Zhou M, et al. Quantification of carotid plaque elasticity and intraplaque neovascularization using contrast-enhanced ultrasound and image registration-based elastography. *Ultrasonics* 2015; 62:253–262
18. Wang X, Jackson DC, Varghese T, et al. Correlation of cognitive function with ultrasound strain indices in carotid plaque. *Ultrasound Med Biol* 2014; 40:78–89
19. Boesen ME, Singh D, Menon BK, Frayne R. A systematic literature review of the effect of carotid atherosclerosis on local vessel stiffness and elasticity. *Atherosclerosis* 2015; 243:211–222
20. Beaussier H, Naggara O, Calvet C, et al. Mechanical and structural characteristics of carotid plaques by combined analysis with echotracking system and MR imaging. *JACC Cardiovasc Imaging* 2011; 4:468–477
21. Doherty JR, Dahl JJ, Kranz PG, et al. Comparison of acoustic radiation force impulse imaging derived carotid plaque stiffness with spatially registered MRI determined composition. *IEEE Trans Med Imaging* 2015; 34:2354–2365
22. Huang C, Pan X, He Q, et al. Ultrasound-based carotid elastography for detection of vulnerable atherosclerotic plaques validated by magnetic resonance imaging. *Ultrasound Med Biol* 2016; 42:365–377
23. Naim C, Cloutier G, Mercure E, et al. Characterisation of carotid plaques with ultrasound elastography: feasibility and correlation with high-resolution magnetic resonance imaging. *Eur Radiol* 2013; 23:2030–2041
24. Grant EG, Benson CB, Moneta GL, et al. Carotid artery stenosis: gray-scale and Doppler US diagnosis—Society of Radiologists in Ultrasound Consensus Conference. *Radiology* 2003; 229:340–346
25. North American Symptomatic Carotid Endarterectomy Trial Collaborators. Beneficial effect of carotid endarterectomy in symptomatic patients with high-grade carotid stenosis. *N Engl J Med* 1991; 325:445–453
26. van der Geest R, Kitslaar P, de Koning P, et al. Advanced three-dimensional postprocessing in computed tomographic and magnetic resonance angiography. In: Ho VB, Reddy GP, eds. *Cardiovascular imaging*. St Louis, MO: Saunders/Elsevier, 2011: 1128–1143
27. Saam T, Ferguson MS, Yarnykh VL, et al. Quantitative evaluation of carotid plaque composition by in vivo MRI. *Arterioscler Thromb Vasc Biol* 2005; 25:234–239
28. Yuan C, Mitsumori LM, Ferguson MS, et al. In vivo accuracy of multispectral magnetic resonance imaging for identifying lipid-rich necrotic cores and intraplaque hemorrhage in advanced human carotid plaques. *Circulation* 2001; 104:2051–2056
29. Naim C, Douziech M, Therasse E, et al. Vulnerable atherosclerotic carotid plaque evaluation by ultrasound, computed tomography angiography, and magnetic resonance imaging: an overview. *Can Assoc Radiol J* 2014; 65:275–286
30. Gupta A, Baradaran H, Schweitzer AD, et al. Carotid plaque MRI and stroke risk: a systematic review and meta-analysis. *Stroke* 2013; 44:3071–3077
31. Fleiner M, Kummer M, Mirlacher M, et al. Arterial neovascularization and inflammation in vulnerable patients: early and late signs of symptomatic atherosclerosis. *Circulation* 2004; 110:2843–2850
32. Millon A, Boussel L, Brevet M, et al. Clinical and histological significance of gadolinium enhancement in carotid atherosclerotic plaque. *Stroke* 2012; 43:3023–3028
33. Destrempes F, Meunier J, Giroux MF, Soulez G, Cloutier G. Segmentation of plaques in sequences of ultrasonic B-mode images of carotid arteries based on motion estimation and a Bayesian model. *IEEE Trans Biomed Eng* 2011; 58:2202–2211
34. Mercure E, Destrempes F, Roy Cardinal MH, et al. A local angle compensation method based on kinematics constraints for non-invasive vascular axial strain computations on human carotid arteries. *Comput Med Imaging Graph* 2014; 38:123–136
35. Wilcox RR. *Introduction to robust estimation and hypothesis testing*. Oxford, UK: Academic Press, 2012
36. Schaar JA, de Korte CL, Mastik F, et al. Characterizing vulnerable plaque features with intravascular elastography. *Circulation* 2003; 108:2636–2641
37. Svedlund S, Eklund C, Robertsson P, Lomsky M, Gan LM. Carotid artery longitudinal displacement predicts 1-year cardiovascular outcome in patients with suspected coronary artery disease. *Arterioscler Thromb Vasc Biol* 2011; 31:1668–1674
38. Zahnd G, Vray D, Sérusclat A, et al. Longitudinal displacement of the carotid wall and cardiovascular risk factors: associations with aging, adiposity, blood pressure and periodontal disease independent of cross-sectional distensibility and intima-

media thickness. *Ultrasound Med Biol* 2012; 38:1705–1715

39. Majdouline Y, Ohayon J, Keshavarz-Motamed Z, et al. Endovascular shear strain elastography for the detection and characterization of the severity of atherosclerotic plaques: in vitro validation and in vivo evaluation. *Ultrasound Med Biol* 2014; 40:890–903
40. Soulez G, Lerouge S, Allard L, et al. Vulnerable carotid atherosclerotic plaque creation in a swine model: evaluation of stenosis creation using absorbable and permanent suture in a diabetic dyslipidemic model. *J Vasc Interv Radiol* 2012; 23:1700.e4–1708.e4
41. Keshavarz-Motamed Z, Saijo Y, Majdouline Y, Riou L, Ohayon J, Cloutier G. Coronary artery atherectomy reduces plaque shear strains: an endovascular elastography imaging study. *Atherosclerosis* 2014; 235:140–149
42. Touzé E, Toussaint JF, Coste J, et al. Reproducibility of high-resolution MRI for the identification and the quantification of carotid atherosclerotic plaque components: consequences for prognosis studies and therapeutic trials. *Stroke* 2007; 38:1812–1819
43. van Wijk DF, Strang AC, Duivenvoorden R, et al. Increasing the spatial resolution of 3T carotid MRI has no beneficial effect for plaque component measurement reproducibility. *PLoS One* 2015; 10:e0130878

FOR YOUR INFORMATION

This article is available for CME and Self-Assessment (SA-CME) credit that satisfies Part II requirements for maintenance of certification (MOC). To access the examination for this article, follow the prompts associated with the online version of the article.

A data supplement for this article can be viewed in the online version of the article at: www.ajronline.org.

Downloaded from www.ajronline.org by Nathalie Bureau on 06/28/17 from IP address 206.167.168.128. Copyright ARRS. For personal use only; all rights reserved